Journal of Power Sources 211 (2012) 129–132

Contents lists available at SciVerse ScienceDirect

Journal of Power Sources

journal homepage: www.elsevier.com/locate/jpowsour

Short communication

3D tin anodes prepared by electrodeposition on a virus scaffold

Xilin Chen [a,1], Juchen Guo [a], Konstantinos Gerasopoulos [b,c], Alex Langrock [a], Adam Brown [d], Reza Ghodssi [b,c,e], James N. Culver [d], Chunsheng Wang [a,*]

[a] Department of Chemical and Biomolecular Engineering, University of Maryland, College Park, MD 20742, USA
[b] Department of Materials Science and Engineering, University of Maryland, College Park, MD 20742, USA
[c] Institute for Systems Research, University of Maryland, College Park, MD 20742, USA
[d] Institute for Bioscience and Biotechnology Research, Department of Plant Science and Landscape Architecture, University of Maryland, College Park, MD 20742, USA
[e] Department of Electrical and Computer Engineering, University of Maryland, College Park, MD 20742, USA

ARTICLE INFO

Article history:
Received 26 January 2012
Received in revised form
18 March 2012
Accepted 19 March 2012
Available online 10 April 2012

Keywords:
Electrodeposition
Tin anode
Lithium-ion battery
Tobacco mosaic virus
3-Dimensional current collector

ABSTRACT

A patterned core–shell tin (Sn) nanorod anode is fabricated by pulse electrodeposition of Sn onto a self-assembled *Tobacco Mosaic Virus* (TMV) structured nickel current collector. Pulse electrodeposition onto the virus assembled 3D electrode surfaces produces homogenous Sn coatings with significant void space to accommodate the large volume change associated with Sn lithiation. The TMV enabled 3D Sn anodes shows high capacity retention of 560 mAh g^{-1} after 100 cycles with the average capacity fading rate of 0.4% per cycle. The high electronic conductivity of Sn, short diffusion length for Li-ions, and large interface between Sn nano-rods and electrolyte greatly enhance the rate performance of the TMV enabled Sn anodes.

1. Introduction

The ability of lithium to electrochemically alloy/dealloy with numerous metals M (M = Mg, Ca, Al, Si, Ge, Sn, Pb, As, Sb, Bi, Pt, Ag, Au, Zn, etc.) [1,2] have made it a favored component for the production of rechargeable batteries.

$$xLi^{+} + xe^{-} + M \underset{\text{charge}}{\overset{\text{discharge}}{\rightleftharpoons}} Li_xM \quad (1)$$

In addition, the high potential capacity for many of these lithium-hosting metals has the potential to significantly improve the capacity and function of existing lithium-ion battery technology. Among these metals, tin (Sn) has attracted extensive attention due to its high capacity of 959.5 mAh g^{-1} [3] which is much higher than graphite anode (372 mAh g^{-1}). However, tin suffers from low Coulombic efficiency and fast capacity fading due to pulverization of the electrode surface resulting from the high volume change (356.4%) that occurs during lithiation. The low Coulombic efficiency but high capacity of Sn anodes will cause quick capacity decline of a full cell. In the past few decades, various technologies have been employed to accommodate the volume change of Sn, thus enhancing its cycling stability. The most successful strategy has been used to decrease the Sn size to a nano-scale or in situ form a Sn/Li_2O composite. Examples include, SnO_2 nanowires [4–6], SnO_2/Sn carbon core–shell nano-spheres [7], silicon coated SnO_2 nanotubes [8], Sn or SnO encapsulated in hollow carbon nano-spheres [9,10], Sn encapsulated in mesoporous carbon [11], Sn or SnO_2 encapsulated in carbon fibers or carbon tubes [12–14], and Sn thin film [15–18]. With these nano-structured Sn materials, the cycling stability as well as capacity has been greatly enhanced.

Electrodeposition of Sn represents a low cost and highly efficient means of synthesizing Sn-based anode materials. To date, only a very limited number of studies have attempted to fabricate Sn anodes via electrodeposition technique [15–18]. Among these previous studies, Hassoun et al. [15] electrochemically deposited metallic Sn onto a copper current collector with various deposition current and time resulting in a modest increase in capacity and cycle stability. Park et al. [16] incorporated carbon particles into the electrodeposited Sn electrode, and Zhao et al. [17] incorporated carbon nanotubes and copper fibers into the electrodeposited Sn. In another study, Zhao and coworkers [18] electrochemically deposited Sn in a porous carbon matrix yielding a higher capacity and

* Corresponding author. Tel.: +1 301 405 0352; fax: +1 301 314 0523.
E-mail address: cswang@umd.edu (C. Wang).
[1] Present address: Pacific Northwest National Laboratory, Richland, WA 99354, USA.

0378-7753/$ – see front matter © 2012 Elsevier B.V. All rights reserved.
doi:10.1016/j.jpowsour.2012.03.070

better cycle stability than the non-patterned electrodeposited Sn anodes.

In this study, to further explore the electrodeposition technique to synthesize Sn anode with improved cyclic stability, Sn was electrodeposited onto a *Tobacco mosaic virus* (TMV) structured 3D current collector. TMV is a high aspect ratio cylindrical plant virus with a length of 300 nm, an outer diameter of 18 nm, and an inner diameter of 4 nm. Genetically modifying the TMV (denoted as TMV1cys) with cysteine residues (amino acids with thiol groups) in its coat protein enables self-assembly of 3D TMV arrays onto stainless steel surfaces due to strong, covalent-like interactions between the thiol groups of the cysteines and metal ions [19]. The genetically introduced thiol groups also enable metal coating, typically nickel, on the TMV1cys surface in electroless plating solution. After the nickel coating, the nickel-coated TMV1cys array on stainless steel substrate serves as a 3D current collector. We have successfully deposited pure Si and n-type Si on the Ni/TMV1cys current collector, and these Si/Ni/TMV1cys anodes demonstrated exceptional cycling stability [20–22]. However, the low electronic conductivity of Si still limited the rate performance of Si/Ni/TMV1cys anodes. Our findings show that Sn deposited on Ni/TMV1cys current collector displays both enhanced cycling stability and increased rate capability.

2. Experimental

The detailed process for the fabrication of nickel-coated TMV1cys current collectors was previously presented [20–22]. Sn was electrochemically deposited onto the TMV1cys enabled 3D current collector from an aqueous solution (0.044 M tin dichloride, 0.22 M triammonium citrate) in a two-electrode cell [23]. Platinum was used as the counter electrode and the 3D current collector acted as the working electrode. A constant pulse current, 2 mA cm^{-2} (2 ms on and 8 ms off), was applied for electrochemical deposition to form a patterned 3D tin anode. Tin dichloride was reduced electrochemically by the following reactions.

$$Sn^{2+} + 2e^- = Sn\downarrow (\text{Working electrode}) \quad (2)$$

$$2Cl^- - 2e^- = Cl_2\uparrow (\text{Counter electrode}) \quad (3)$$

With the additive, triammonium citrate, tin dichloride is able to be stabilized in the neutral aqueous solution for a long time [23]. There are two advantages to use tin dichloride for electrodeposition. The first one is that the reaction ($Sn^{2+} + 2e^- = Sn\downarrow$) occurring in the neutral plating bath involves two electrons instead of four electrons found in the basic plating solution ($SnO_3^{2-} + 4e^- + 3H_2O = Sn\downarrow + 6OH^-$). This indicates that the efficiency in the neutral aqueous plating solution is doubled compared with using the basic plating solution. The second advantage is that the plating bath used in this work does not need to be heated to get better deposition morphology, unlike the basic plating bath. This feature makes the electrodeposition setup less complex and easy to control.

The amount of electrodeposited Sn was determined by measuring the weight difference of Ni/TMV1cys before and after Sn electrodeposition and by calculation based on Faraday's law. The efficiency of electrodeposition is very close to 100%. The amount of deposited tin on the electrode is about 0.7 mg cm^{-2}. The patterned 3D tin anodes were characterized using scanning electron microscopy (Hitachi SU-70 HR-SEM with energy-dispersive X-ray spectroscopy (EDS)) and transmission electron microscopy (JEOL 2100F field emission TEM). The electrochemical performance of patterned Sn anodes is tested in coin cells using lithium metal as the counter electrode and 1M $LiPF_6$ in ethylene carbonate/diethyl carbonate (1:1) as electrolyte. The charge/discharge behaviors of Sn anodes were investigated using an Arbin BT2000 battery test station at 1 A g^{-1} charge/discharge current density. The Li insertion/extraction kinetics of Sn anodes was also characterized by electrochemical impedance spectroscopy (EIS) and cyclic voltammetry (CV) techniques using the Solartron 1260/1287 electrochemical interface. 10 mV voltage amplitude and a frequency range of 1 MHz and 0.005 Hz were used in EIS test and 0.2 mV s^{-1} scan rate was used in CV test.

3. Results and discussion

Fig. 1a shows the SEM image of the TMV1cys structured Sn anode after electrodeposition, and the TEM image of a single Sn/Ni/TMV1cys nanorod is shown in Fig. 1b. The diameter of the TMV1cys core is ~18 nm, the thickness of the Ni shell is also ~18 nm, and the thickness of the Sn layer is ~10 nm. The rod shaped TMV1cys particles are known to form end to end self associations leading to Ni/TMV1cys lengths that vary from 300 nm for a single TMV1cys to 900 nm for three aligned particles [20,21]. Fig. 1b also shows the elemental distribution in the radial direction in a single nanorod.

The prepared 3D Sn anode was characterized by XRD to investigate the structure of the Sn layer. As shown in Fig. 2, the peaks of crystalline Sn (PCPDF# 040673) and Ni–Sn alloy were found in the XRD pattern. The Ni–Sn alloy is formed on the interface between Ni and Sn layers at the beginning of Sn layer growth. This Ni–Sn alloy does not affect the capacity of tin because Ni–Sn alloy is able to

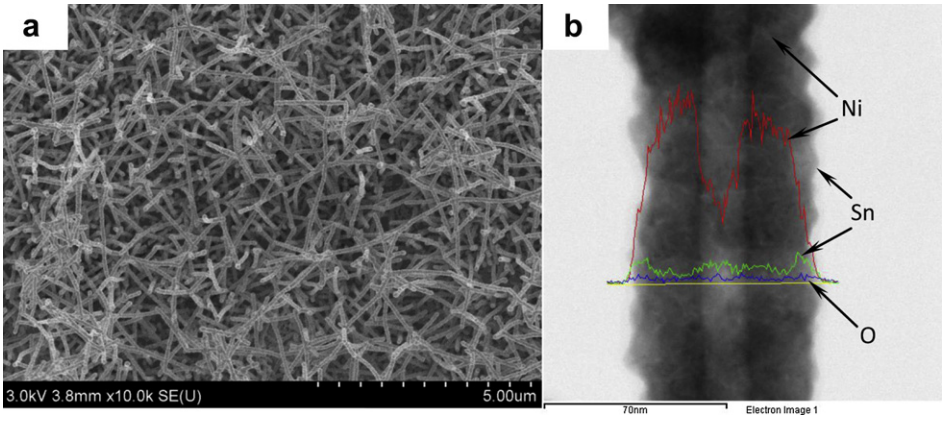

Fig. 1. (a) SEM image after tin electrodeposition and (b) TEM image with XDS patterns of a single Sn/Ni/TMV1cys nanorod.

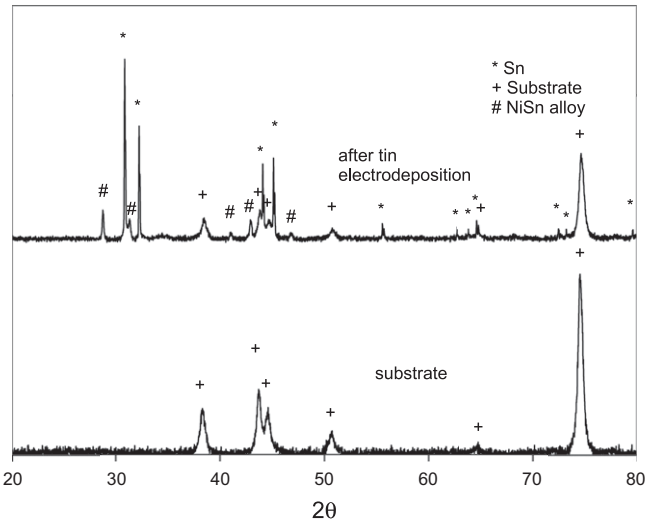

Fig. 2. XRD patterns of the 3D tin anode and bare substrate.

react with lithium to form Ni metal and Li_xSn alloy [24]. The formation of Ni–Sn alloy enhanced the bonding between Si and Ni substrate, which improved the cycling stability and rate capability.

The electrochemical performance of the 3D tin anode was tested in 2032 coin cells using lithium metal as the counter electrode. The CV curves recorded at a scan rate of 0.2 mV s^{-1} between 0 and 2.0 V are shown in Fig. 3a. The first CV cycle shows a broad reduction peak located at 1.2 V, which disappears during the second and third cycles. It is well known that Li_xSn formation does not occur above 0.8 V [4–6]. The peak at 1.2 V has been attributed to the catalytic decomposition of electrolyte on Sn surface [25–28]. All other peaks in the CV curve are typical for a Sn anode and consistent with the literature [22,24,29,30]. The corresponding charge–discharge plateaus were also found in the charge–discharge curves as shown in Fig. 3b. As seen in Fig. 3b, the initial irreversible capacity is ~36%, which is lower than those reported in literature for electrodeposited Sn anode [17]. The main irreversible capacity results from the formation of a solid electrolyte interphase (SEI) film. The oxidized Sn/Ni (oxygen was found by EDS as shown in Fig. 1b) also has a contribution to the irreversible capacity.

Fig. 4 shows the cyclic stability and the corresponding coulombic efficiency for the 3D Sn anode cycled between 0 and 1.5 V. The first discharge capacity is 1308 mAh g^{-1} and the first charge capacity is 930 mAh g^{-1}. Here, the discharge process corresponds to lithiation process and the charge process corresponds to delithiation process of Tin electrodes. The initial charge capacity is very close to the theoretical capacity (~959.5 mAh g^{-1}) of Sn. The coulombic efficiency quickly increases from the initial 64% in the first cycle to above 99% by 20 cycles and then stabilized around 99.7% after 30 cycles. At 100 cycles, the retained capacity is about 560 mAh g^{-1}. The capacity decrease per cycle is approximately 0.4%. The stability of this TMV1cys structured 3D tin anode is much better than the previously reported electrochemically deposited Sn anodes [15–18]. The superior capacity retention and coulombic efficiency of TMV1cys structured Sn anode shows that the nickel core inside each tin tubular shell significantly improves the structural integrity of the anode. The large contact area between tin and nickel (current collector) favors both uniform lithium insertion and extraction. In addition, the void space in the 3D structure is very efficient in reducing the stress and preventing pulverization at the Sn anode surface during lithiation and delithiation processes. These attributes are thus responsible for the observed stability of the anode during repeated cycling.

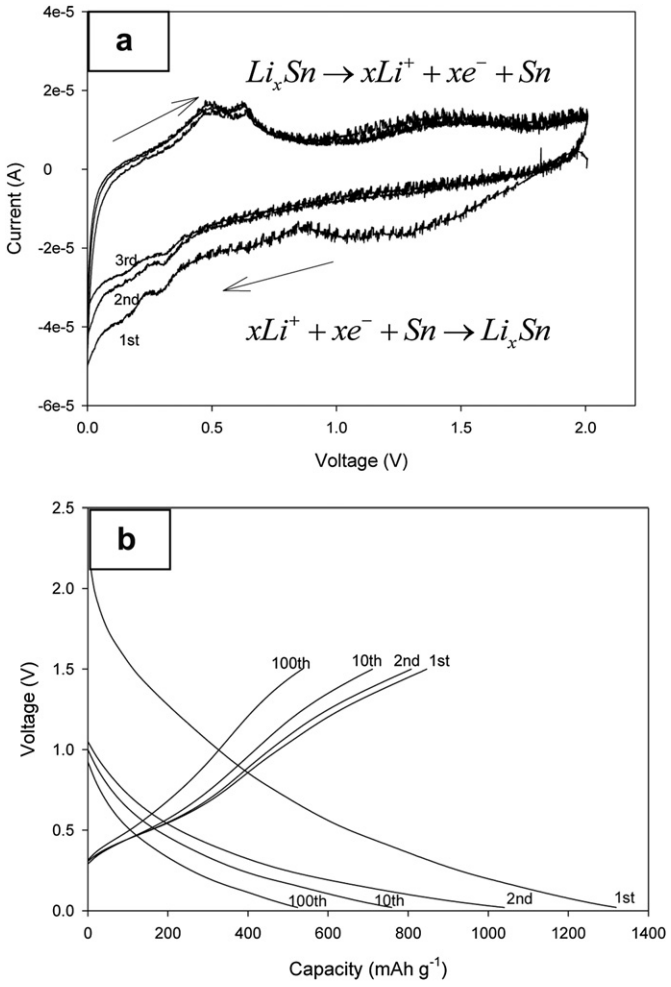

Fig. 3. (a) Cyclic voltammograms at 0.2 mV s^{-1} and (b) charge-discharge curves at 1A g^{-1} current of Sn/Ni/TMV1cys anode.

Fig. 5 shows the impedance of the patterned electrodeposited tin on Ni/TMV1cys 3D current collector after different cycles. The impedance was measured after the tin was fully lithiated. All the impedance spectra have similar features: a depressed semicircle at medium-to-high frequency range and an inclined line at low

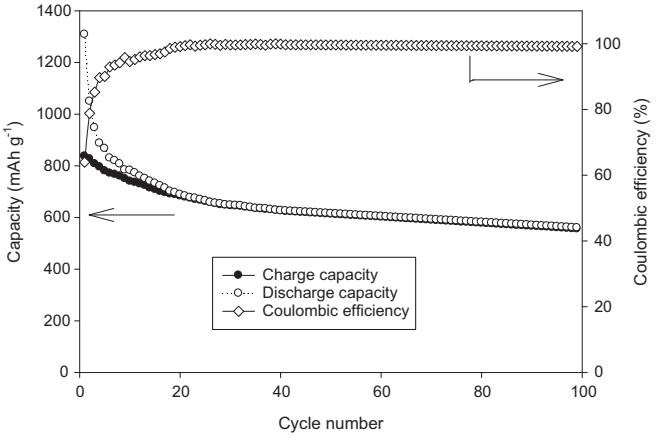

Fig. 4. Stability of the 3D tin anode at 1A g^{-1} using lithium metal as counter electrode and 1M $LiPF_6$ in EC/DEC (1:1) as electrolyte.

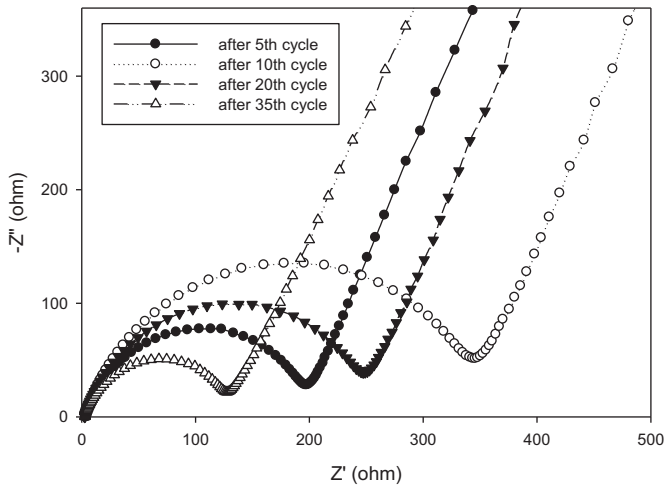

Fig. 5. Impedance study of the 3D tin anode using lithium metal as counter electrode and 1M $LiPF_6$ in EC/DEC (1:1) as electrolyte.

frequency, which is in good agreement with previously reported impedance spectra of tin anode [17,31]. The inclined line in the low frequency region represents the lithium diffusion impedance, while the depressed semicircle is attributed to the overlap between the SEI film and the interfacial charge transfer impedance. Impedance studies reveal that the total SEI and charge transfer resistances increase at first, and then decrease after the 10th cycle. Similar to Si/Ni/TMV1cys anodes [20], the improved kinetics of the charge/discharge cycles may be attributed to increased tin porosity resulting from repeated volume changes that occur during lithium insertion/extraction.

The unique 3D substrate architecture of this anode, the high electronic conductivity of the nickel core, and the integrity of the nickel core and tin shell in our electrodeposited tin anode combine to produce a novel anode with enhanced rate performance. As shown in Fig. 6, the TMV1cys structured Sn anode was cycled at various current densities. At each current density, the battery was tested for 20 cycles. The electrodeposited tin shows an average capacity of 750 mAh g^{-1}, 370 mAh g^{-1}, 150 mAh g^{-1}, 30 mAh g^{-1} at 1 A g^{-1}, 2 A g^{-1}, 4 A g^{-1}, 8 A g^{-1}, respectively. The average capacity of the Sn anode decreases from 750 mAh g^{-1} to 370 mAh g^{-1} with increasing current density from 1 A g^{-1} to 2 A g^{-1}. This rate

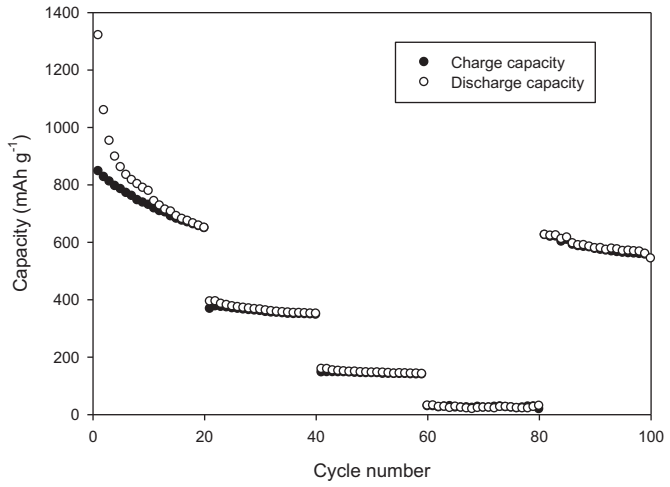

Fig. 6. Rate performance of the 3D tin anode using lithium metal as counter electrode and 1M $LiPF_6$ in EC/DEC (1:1) as electrolyte.

capability is much higher than other electrodeposited tin [15–18] or graphite-tin composites [30]. The improved rate capability of our electrodeposited Sn anode can be attributed to the electronic conductivity of the Sn shell and nickel core.

4. Conclusion

A patterned 3D Sn anode is fabricated by electrodepositing Sn on a self-assembled TMV1cys structured nickel current collector in a neutral aqueous solution. The large amount of void space among this unique nano-patterned 3D current collector provides the electrodeposited Sn anode with excellent stability. The retention of capacity is 560 mAh g^{-1} after 100 cycles and the average capacity fading rate is 0.4%. The rate performance investigation shows a 370 mAh g^{-1} capacity at 2 A g^{-1}.

Acknowledgment

The authors acknowledge financial support from the Department of Energy (DESC0001160) under the project science of precision multifunctional nanostructures for electrical energy storage, and the technical support of the Maryland NanoCenter. Dr. Culver also acknowledges the support of the Department of Energy, the Office of Basic Energy Sciences DEFG02-02-ER45975.

References

[1] A.N. Dey, J. Electrochem. Soc. 118 (1971) 1547–1549.
[2] M. Winter, J.O. Besenhard, Electrochim. Acta 45 (1999) 31–50.
[3] C. Park, J. Kim, H. Kim, H. Sohn, Chem. Soc. Rev. 39 (2010) 3115–3141.
[4] N. Li, C.R. Martin, J. Electrochem. Soc. 148 (2001) A164–A170.
[5] M. Park, G. Wang, Y. Kang, D. Wexler, S. Dou, H. Liu, Angew. Chem. Int. Ed. 46 (2007) 750–753.
[6] P. Meduri, C. Pendyala, V. Kumar, G.U. Sumanasekera, M. Sunkara, Nano Lett. 9 (2009) 612–616.
[7] D. Deng, J.Y. Lee, Chem. Mater. 20 (2008) 1841–1846.
[8] W.J. Lee, M. Park, Y. Yang, J.Y. Lee, J. Cho, Chem. Commun. 46 (2010) 622–624.
[9] W. Zhang, J. Hu, Y. Guo, S. Zheng, L. Zhong, W. Song, L. Wu, Adv. Mater. 20 (2008) 1160–1165.
[10] X. Lou, D. Deng, J. Lee, L.A. Archer, Chem. Mater. 20 (2008) 6562–6566.
[11] G. Derrien, J. Hassoun, S. Panero, B. Scrosati, Adv. Mater. 19 (2007) 2336–2340.
[12] Y. Yu, L. Gu, C. Wang, A. Dhanabalan, P.A. van Aken, J. Maier, Angew. Chem. Int. Ed. 48 (2009) 6485–6489.
[13] Y. Yu, L. Gu, C. Zhu, P.A. van Aken, J. Maier, J. Am. Chem. Soc. 131 (2009) 15984–15985.
[14] Y. Wang, M. Wu, Z. Jiao, J. Lee, Chem. Mater. 21 (2009) 3210–3215.
[15] J. Hassoun, S. Panero, P. Reale, B. Scrosati, Int. J. Electrochem. Sci. 1 (2006) 110–121.
[16] J. Park, J. Eom, H. Kwon, Electrochem. Commun. 11 (2009) 596–598.
[17] X. Zhang, Z. Xia, D. Xia, Electrochim. Acta 55 (2010) 6004–6009.
[18] H. Zhao, C. Jiang, X. He, J. Ren, C. Wan, Electrochim. Acta 52 (2007) 7820–7826.
[19] S. Lee, E. Royston, J.N. Culver, M.T. Harris, Nanotechnology 16 (2005) S435–S441.
[20] X. Chen, K. Gerasopoulos, J. Guo, A. Brown, C. Wang, R. Ghodssi, J.N. Culver, ACS Nano 4 (2010) 5366–5372.
[21] X. Chen, K. Gerasopoulos, J. Guo, A. Brown, C. Wang, R. Ghodssi, J.N. Culver, Adv. Funct. Mater. 21 (2007) 380–387.
[22] X. Chen, K. Gerasopoulos, J. Guo, A. Brown, C. Wang, R. Ghodssi, J.N. Culver, Electrochim. Acta 56 (2011) 5210–5213.
[23] A. He, Q. Liu, D.J. Ivey, J. Mater. Sci. Mater. Electron. 19 (2008) 553–562.
[24] M. Wachtler, M. Winter, J.O. Besenhard, J. Power Sources 105 (2002) 151–160.
[25] N. Tamura, R. Ohshita, M. Fujimoto, S. Fujitani, M. Kamino, I. Yonezu, J. Power Sources 107 (2002) 48–55.
[26] L.Y. Beaulieu, S.D. Beattie, T.D. Hatchard, J.R. Dahn, J. Electrochem. Soc. 150 (2003) A419–A424.
[27] S.D. Beattie, T. Hatchard, A. Bonakdarpour, K.C. Hewitt, J.R. Dahn, J. Electrochem. Soc. 150 (2003) A701–A705.
[28] N. Pereira, L.C. Klein, G.G. Amatucci, Solid State Ionics 167 (2004) 29–40.
[29] C. Li, W. Ho, C. Jiang, C. Lai, M. Wang, S. Yen, J. Power Sources 196 (2011) 768–775.
[30] J. Xie, N. Imanishi, A. Hirano, Y. Takeda, O. Yamamoto, X.B. Zhao, G.S. Cao, Solid State Ionics 181 (2010) 1611–1615.
[31] F. Nobili, M. Mancini, S. Dsoke, R. Tossici, R. Marassi, J. Power Sources 195 (2010) 7090–7097.